PCCP

ROYAL SOCIETY OF CHEMISTRY

PAPER

Check for updates

Cite this: *Phys. Chem. Chem. Phys.*, 2021, **23**, 1520

Radical pair formation due to compression-induced electron transfer in crystals of energetic salts†

Sergey V. Bondarchuk

Received 26th October 2020,
Accepted 12th December 2020

DOI: 10.1039/d0cp05587e

rsc.li/pccp

An interesting effect was observed when studying explosive and non-explosive crystalline ionic materials at high pressures. A wide benchmark set of 76 crystals of different families was studied using the state-of-the-art methods at ambient pressure and in extremes (at 20, 50 and 100 GPa). It was found that hydrostatic compression leads to an electron transfer from the anion to the cation, which was carried out with different efficiencies for explosive and non-explosive salts. The measure of this electron transfer is reflected in the Hirshfeld charges (q) on cations, which decreased with the rise of pressure. Non-explosive materials are generally resistant to this effect, while explosives are much more susceptible. Thus, at 100 GPa, all the studied energetic salts demonstrate $q_{cat} < +0.1e$, while for the non-explosive salts $q_{cat} > +0.1e$. This value can be considered as a conditional boundary between explosive and non-explosive salts. The observed effect is in accord with the Szigeti's dielectric theory as well as with the electrophilicity/electronegativity equalization principle. In the present paper, we develop a mechanism of the explosive decomposition based on the assumption about formation of a radical pair as a result of the following reaction: $Cat^{+} + An^{-} \overset{\text{Pressure}}{\rightleftharpoons} Cat^{\bullet} + An^{\bullet}$. The study of such radicals revealed their intrinsic instability, which generally reflects either in a dissociative structure or in the presence of strongly weakened trigger bonds.

Introduction

High-pressure chemistry demonstrates sustainable development due to interesting and often unexpected changes in chemical properties of the elements.[1] A recently developed model for simulation of an isotopic compression of atoms has shown drastic changes to ground-state electronic configurations and electronegativity in the pressure range of 0–300 GPa.[2] Moreover, hydrostatic compression leads to the stress-redox equivalence in crystals caused by the change in electronegativity.[3] Such a redox process has been recently observed in a viologen–carboxylate zwitterionic molecule, which demonstrates a piezochromic nature due to the compression-induced electron transfer.[4] Apart from the reversible electron transfer, like in the previous case, there are examples of an irreversible redox reaction in the transition metal complexes ($Cs_2PdI_4{\cdot}I_2$, and $Cs_2Au^{I}Au^{III}Cl_6$) leading to compounds with the same empirical formula but with different oxidation states of the transition metals.[5,6] Moreover, compression-induced charge transfer was also observed in the graphene/MoS_2 heterostructure[7] and $LaNi_{0.5}Fe_{0.5}O_3$.[8]

Such changes in electronic structure and reactivity can be explained in terms of the well-known electronegativity equalization principle[9–11] or other molecular properties obtained in terms of conceptual density functional theory (DFT), like electrophilicity (eqn (1)).[12] Indeed, when two atoms with different electronegativity (χ) form a molecule, the higher value decreases and the lower one increases. Since χ is the negative of chemical potential of the electronic cloud (μ), which is constant throughout the molecule, χ changes to a common intermediate value.[10]

$$\chi = -\mu = -\left(\frac{\partial E}{\partial N}\right)_{\nu(\mathbf{r})} \quad (1)$$

This situation is consistent with the process of electron loss by the less electronegative atom and thus forming a covalent polar or an ionic bond. Thereafter, effective electronegativity of the atom i in a molecule can be expressed as in eqn (2):[13]

$$\chi_i = A_i + B_i q_i + \kappa \sum_{j=1(j\neq i)}^{N} \frac{q_j}{R_{i,j}} \quad (2)$$

where N is the number of atoms in the molecule; $R_{i,j}$ is the distance between atoms i and j; q_i and q_j are the charges on

Department of Chemistry and Nanomaterials Science, Bogdan Khmelnitsky Cherkasy National University, blvd. Shevchenko 81, 18031 Cherkasy, Ukraine. E-mail: bondchem@cdu.edu.ua

† Electronic supplementary information (ESI) available: Chemical formulas and full names, crystal structures, asymmetric cell parameters, relative errors, partial charges at different pressures, frontier molecular orbital energies and decomposition equations. See DOI: 10.1039/d0cp05587e

This journal is © the Owner Societies 2021

atoms i and j; κ, A_i and B_i are, respectively, empirical parameters, which can be done as in eqn (3):

$$A_i = \chi_i^0 + \Delta\chi_i \text{ and } B_i = 2(\eta_i^0 + \Delta\eta_i). \quad (3)$$

Herein, χ_i^0 and η_i^0 are the electronegativity and hardness of an isolated neutral atom, respectively; $\Delta\chi_i$ and $\Delta\eta_i$ are structure-dependent parameters.[13] It is obvious that equalization of χ directly affects atomic charges q.

Now, let us consider what processes occur in an ionic crystal. At ambient pressure, cations and anions are fixed at their equilibrium positions, which correspond to ionic distances. Note that the cation now has a higher χ than the anion. The effective ionic charge in a crystal can be obtained by the second Szigeti's relation (eqn (4)):[14,15]

$$qs = \omega_T\left(\frac{\varepsilon_0 - \varepsilon_\infty}{4\pi}\right)^{1/2}\frac{3}{\varepsilon_\infty + 2}(\mu V_a)^{1/2}, \quad (4)$$

where ε_0 and ε_∞ are the static dielectric constants and the corresponding value at frequency $\omega \gg \omega_T$ (ω_T is the transverse optical frequency); μ is the reduced mass; V_a is the volume per ion pair; $s \leq 1$.

When hydrostatic compression is applied to a crystal, it decreases its volume forcing ions to move towards each other. Again, this causes equalization of electronegativity,[16–18] but in this case, the cation tends to pull the valence electrons back to weaken the effect of bond polarity on the resisting ability to volume compression.[19] Expression of the effect of asymmetry distribution of valence electrons can be done *via* the effective ionicity (f_e) as in eqn (5):[19]

$$f_e = \frac{\chi_b - \chi_a}{Z_a(\chi_a + \chi_b)}, \quad (5)$$

where Z_a is the valence state of the cation.

Pressure-dependence of the effective ionic charge can be obtained by differentiation of eqn (4) with respect to pressure (eqn (6)).[15]

$$\frac{d\ln s}{d\ln V} = \frac{-1}{2\chi_T}\left\{\frac{1}{\varepsilon_0 - \varepsilon_\infty}\left[\left(\frac{d\varepsilon_0}{dp}\right)_T - \left(\frac{d\varepsilon_\infty}{dp}\right)_T\right] - \frac{2}{\varepsilon_\infty + 2}\left(\frac{d\varepsilon_\infty}{dp}\right)_T - \chi_T\left[1 + 2\left(\frac{d\ln\omega_T}{d\ln V}\right)_T\right]\right\}, \quad (6)$$

This results in deviation of s from 1 (typically, $s < 1$) due to the ionic distortion caused by mutual interaction of neighboring ions increasing with compression.[15] Thus, an important conclusion follows from the Szigeti's dielectric theory that the decrease in crystal volume due to compression increases overlap and distortion of ions, thereby causing a decrease in the effective ionic charge.[20] Therefore, in this paper, we have tried to find out how ionic charges are changed for explosive and non-explosive salts using first-principles calculations.

Computational details

The calculations of periodic systems were performed in terms of density functional theory (DFT) using the Cambridge Serial Total Energy Package (CASTEP) code[21] implemented in the Materials Studio 2017 program suite.[22] "On-the-fly" generated norm-conserving (OTFG NC) pseudopotentials with the states H-$1s^1$, Li-$1s^22s^1$, Na-$2s^22p^63s^1$, K-$3s^23p^64s^1$, Rb-$4s^24p^65s^1$, Ca-$3s^23p^64s^2$, Ba-$4s^24p^65s^2$, Ti-$3s^23p^63d^24s^2$, Fe-$3s^23p^63d^64s^2$, Ag-$4s^24p^64d^{10}5s^1$, Al-$3s^23p^1$, Tl-$5d^{10}6s^26p^1$, Pb-$5d^{10}6s^26p^2$, C-$2s^22p^2$, N-$2s^22p^3$, O-$2s^22p^4$, F-$2s^22p^5$, P-$3s^23p^3$, S-$3s^23p^4$, Cl-$3s^23p^5$, Br-$3d^{10}4s^24p^5$ and I-$5s^25p^5$ treated as the valence electrons were applied entirely in this work. Cell relaxations were performed using pure GGA functional due to Perdew–Burke–Ernzerhof (PBE).[23] Wave functions were expanded in a plane wave basis set with an energy cutoff, which depends on the convergence test for each element.[22] These are as follows: H (540 eV), Li (810 eV), Na (870 eV), K (480 eV), Rb (260 eV), Ca (420 eV), Ba (370 eV), Ti (630 eV), Fe (1440 eV), Ag (900 eV), Al (270 eV), Tl (520 eV), Pb (530 eV), C (720 eV), N (990 eV), O (990 eV), F (840 eV), P (300 eV), S (290 eV), Cl (390 eV), Br (1350 eV) and I (280 eV). Thus, for any combination of these elements, the energy cutoff was determined by the highest value.

Sampling of the Brillouin zones were performed using k-point mesh generated by the Monkhorst–Pack algorithm. Direct spacing between k-points was specified to be 0.08 2πÅ^{-1}. Convergence quality parameters are as follows: total energy (5×10^{-6} eV per atom), force (0.01 eV Å^{-1}), stress (0.02 GPa) and displacement (5×10^{-4} Å). Dispersion effects were taken into account using the Grimme form of the damped C_6 term.[24] The following extra parameters of van der Waals force field have been applied: Ba (C_6 = 2352.6270 eV Å^6, and R_0 = 1.7620 Å), Tl (C_6 = 593.3959 eV Å^6, and R_0 = 1.9890 Å) Pb (C_6 = 654.6280 eV Å^6, and R_0 = 1.9440 Å). The electronic wave functions were obtained by the density mixing scheme.[25] The finite basis set correction was also included entirely. Optimization of the asymmetric cells was performed by means of the Broyden, Fletcher, Goldfarb and Shannon (BFGS) method.[26]

Partial charges were obtained using the Hirshfeld partitioning scheme (eqn (7)):[27]

$$q_A = Z_A - \int \frac{\rho_A(\mathbf{r})}{\rho_{promolecule}(\mathbf{r})}\rho_{molecule}(\mathbf{r})d\mathbf{r} \quad (7)$$

This method is based directly on the electron density as a function of space rather than a representation of the molecular wave function using basis functions, like in the Mulliken population analysis. Unlike the Mulliken, Bader and natural charges, the Hirshfeld and Voronoi deformation density (VDD) schemes yield chemically meaningful charges and are recommended for use.[27] Thus, the main conclusions of this work are drawn on the basis of Hirshfeld population analysis.

The DFT calculations of non-periodic systems were performed using the Gaussian09 program suite.[28] We have used the long-range corrected hybrid functional with damped atom–atom dispersion corrections, namely, ωB97XD[29] along with Pople's split-valence quasi-double-ζ in the valence shell basis set (6-31G). The latter was augmented with both polarization (d,p) and diffuse (+) functions.[30]

Results and discussion

The effect of pressure on the ionic charges

First of all, we have chosen an arbitrary set of explosive and non-explosive salts, which included 65 crystals (salts **1–65**). The only criteria of selection were relatively small molecular size and low Z' crystal structures. As non-explosive species we have selected various metal salts of inorganic (halides, carbonates, sulfate, phosphate, nitrate, *etc.*) and organic (tartrate, citrate, sulfonate, *etc.*) salts, alkoxides, phosphonium salts and so on. Additionally, as explosive crystals, we have chosen salts of nitroaliphatics, nitrogen-containing heterocycles, pentazoles, aryldiazonia, oxadiazole, azide, *etc.* Their chemical formulas, names and crystal structures are presented in Fig. S1 and S2 in the ESI.†

The relaxed *versus* experimental asymmetric cell parameters of the studied salts are listed in Table S1 in the ESI.† As one can see, the applied method provides very good structural results, which are reflected in the low relative errors $\delta = (V_{theor} - V_{exper})/V_{exper}$ of the asymmetric cell volume estimation (Table S2 in the ESI†). Statistical treatment of these data provides the following estimates: mean (−0.13%), median (−0.12%), mode (−2.4%), δ_{max} (9.68%), and δ_{min} (−6.02%). Thus, we can conclude that structures of these salts are reproduced properly.

Graphical description of the pressure-dependence of cationic charges of salts **1–55** is presented in Fig. 1 and the numerical data at each specific pressure are listed in Table 1 and Table S3 in the ESI.† We should stress that salts **56–65** will be discussed independently as their explosive nature cannot be rationalized on the basis of pressure-dependence of ionic charges and/or cell volumes. To provide a strict meaning for terms "explosive" and "non-explosive" we have applied the energy content (E_c) quantity, which is the enthalpy of the decomposition reaction (Table S4 in the ESI†) built in terms

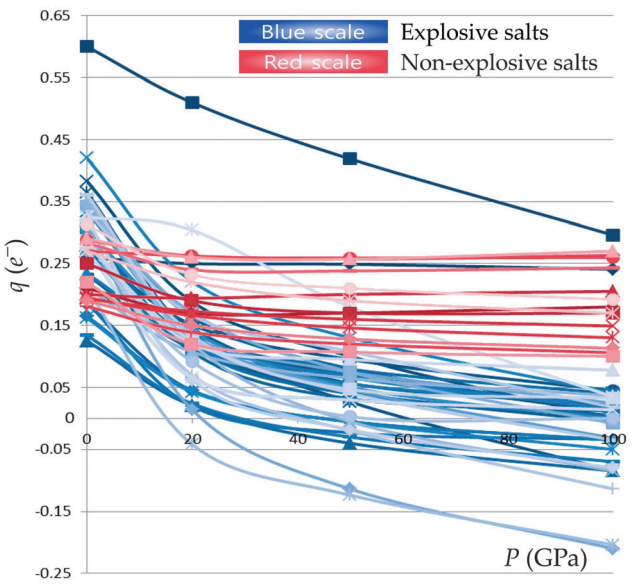

Fig. 1 Pressure-dependence of the Hirshfeld cationic charges of explosive and non-explosive salts.

Table 1 The Hirshfeld cationic charges (q, e^-) at different pressures, unit cell volume ratios (V_0/V_{100}) and energy contents (E_c, kJ mol^{-1} atom^{-1})

Salt	$q_{100} - q_0$	q_{100}	V_0/V_{100}	E_c
1	−0.030	0.180	2.092	−227.0
2	−0.080	0.170	2.375	−218.7
3	0.005	0.205	1.311	−20.5
4	−0.044	0.149	2.024	−30.7
5	−0.065	0.130	1.728	−32.8
6	−0.028	0.260	1.653	−10.9
7	−0.075	0.106	1.635	−58.2
8	−0.007	0.263	1.679	−50.2
9	−0.040	0.243	1.838	−51.3
10	−0.077	0.113	1.813	−27.4
11	−0.120	0.100	1.455	−159.8
12	−0.020	0.270	1.863	−111.3
13	−0.019	0.241	2.036	0.1
14	−0.100	0.170	1.703	−86.3
15	−0.120	0.192	2.218	−58.3
16	−0.304	0.296	2.266	23.8
17	−0.270	0.010	2.114	17.7
18	−0.383	0.000	2.075	47.5
19	−0.449	−0.085	2.033	54.2
20	−0.230	0.045	2.237	0.5
21	−0.277	0.022	1.934	17.4
22	−0.237	−0.005	1.969	26.4
23	−0.333	0.010	1.961	11.6
24	−0.220	−0.035	2.096	5.7
25	−0.296	0.012	1.969	34.0
26	−0.210	−0.085	2.004	16.2
27	−0.305	0.005	2.011	0.8
28	−0.294	0.040	2.004	6.2
29	−0.340	0.003	2.136	19.2
30	−0.221	−0.034	2.196	6.1
31	−0.255	0.015	1.983	3.4
32	−0.204	−0.070	2.045	9.1
33	−0.200	−0.035	2.095	15.0
34	−0.192	0.024	2.018	6.8
35	−0.218	0.016	2.075	6.6
36	−0.379	0.041	2.319	21.1
37	−0.212	−0.050	2.069	1.8
38	−0.305	−0.001	2.020	16.8
39	−0.256	0.014	2.024	28.1
40	−0.369	−0.032	2.068	37.8
41	−0.240	0.025	1.866	32.2
42	−0.520	−0.210	2.060	26.4
43	−0.350	−0.008	2.004	23.3
44	−0.173	0.037	1.968	0.4
45	−0.440	−0.085	1.982	10.7
46	−0.414	−0.204	2.046	20.1
47	−0.283	0.000	1.993	16.8
48	−0.408	−0.114	2.014	23.2
49	−0.316	0.018	2.026	24.5
50	−0.396	−0.035	2.015	29.8
51	−0.399	−0.080	2.068	20.9
52	−0.247	0.033	2.003	30.5
53	−0.207	0.078	2.131	33.9
54	−0.256	0.014	2.008	37.3
55	−0.290	0.035	2.148	33.1

of the well-known [H_2O–CO_2] arbitrary decomposition assumption and normalized per atom.[31,32] The calculations of E_c were done using the plane wave pseudopotential method as described in the Computational details section. This method is necessary since many species in Table S4 (ESI†) are solid crystalline matter, which must be treated using periodic boundary conditions. At the same time, gaseous species were calculated using supercell approximation with separation no shorter than 20 Å for all axes. As a result, salts with positive E_c are considered as

This journal is © the Owner Societies 2021

"explosive", while ones with negative E_c are assumed to be "non-explosive" (Table 1). This quantity safely distinguishes all the salts except sulfonate (**13**) and methoxide (**63**), for which small positive E_c values are predicted. However, it does not mean that these compounds are indeed explosive, since energetic barriers may be too high. Therefore, in this work we strictly follow differentiation of salts based on the E_c values.

As shown in Fig. 1, non-explosive salts demonstrate resistance to the change of ionic charges, while explosive ones are much more sensitive. Though the q_{100} value for tosylate **16** is 0.296 e, its $q_{100} - q_0$ value equals −0.304. Therefore, this salt can be safely distinguished as explosive, despite its curve lying much higher than those of other explosives (Fig. 1). In a number of cases, at 100 GPa the latter demonstrate an inverse polarization with formal negative charges on cations. This is a quite unexpected effect meaning that more than one electron is coming to the cation. This is, probably, caused by the change in electronegativity of the species formed under high pressure. We should stress, however, that q_{100} is an arbitrary value, which should not be considered as a physically meaningful constant. One can apply, say, q_{80} or any other pressure. For example, the values q_{50} can also be effectively applied (Table S3 in the ESI†). Herein, such an extreme pressure is applied only for a clear and obvious differentiation with the naked eye. The physical sense is only in the ease of an electron transfer from an anion to a cation or $\partial q/\partial P$, which is more negative for explosives (see the $q_{100} - q_0$ values in Table 1).

The data from Table 1 for salts **1–55** are displayed graphically in Fig. 2. It is clearly seen that the values of charges and their absolute decrease reproduce the E_c values quite well. Additionally, we have also checked the relative loss of volume under pressure,

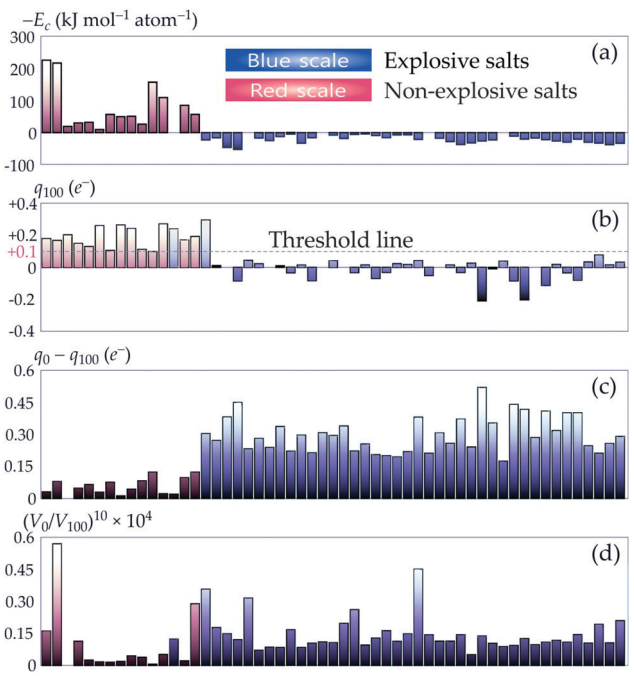

Fig. 2 Energy content (a), cation charge at 100 GPa (b), absolute decrease in charge (c) and relative decrease in volume (d) of salts **1–55**.

Table 2 The salts, whose explosive nature cannot be distinguished on the basis of pressure-dependence of ionic charges and/or cell volumes

Salt	$q_{100} - q_0$	q_{100}	V_0/V_{100}	E_c
56	−0.050	0.080	1.854	−47.1
57	−0.017	0.303	2.151	27.3
58	0.005	0.273	1.734	17.6
59	−0.337	−0.080	1.979	−51.8
60	−0.348	−0.079	2.247	−22.9
61	−0.378	−0.120	2.110	−7.7
62	−0.429	−0.160	2.557	−11.0
63	−0.060	0.145	1.778	3.9
64	−0.040	0.020	1.332	−9.6
65	−0.150	0.129	2.063	37.0

which is a crude representative of bulk modulus of a crystal. Earlier, we have developed a model, in which bulk modulus was shown to be directly proportional to impact energy assuming that non-explosive crystals must be much harder mechanically.[33] Moreover, crystal compressibility (the inverse of the bulk modulus) also correlates with co-called band gap compressibility (β_E), which determines the ability of band gap to close upon pressure.[33,34] The greater the β_E, the greater the impact sensitivity and, hence, the energy content.[35] As shown in Fig. 2d, non-explosive salts generally possess lower V_0/V_{100} values that correspond to higher bulk moduli and are in accord with the above-mentioned model.[33]

Not all of the studied salts, however, demonstrate such a good agreement between q_{100} and $-E_c$ (Table 2). With some exceptions, these are generally azides and non-explosive onium salts (ammonium, and phosphonium). Azides do not demonstrate systematic error, while onium salts always behave as explosives (Table 2). Actually, it is hard to say what the reasons of such errors are. Probably, it can be related to some phase transitions or any other structural changes caused upon compression;[36–43] anyway, this should be the issue of a further more detailed study.

Mechanistic considerations and model calculations

Recently, we have proposed that compression of aryl diazonium crystal salts leads to an electron transfer from anion to cation, which can explain why these salts are explosive, since the corresponding aryl diazenyl radicals are unstable and lose molecular nitrogen.[44] In the present work, we have extended this idea to the other salts, which can be divided into two groups: (1) ones formed due to an electron transfer; (2) ones formed due to a proton transfer (onium salts). Thus, the formation of a salt and the corresponding changes upon crystal compression can be expressed as follows:

$$An^{\bullet} + Cat^{\bullet} \rightarrow An^{-} + Cat^{+} \xrightarrow{\text{Pressure}} An^{\bullet} + Cat^{\bullet}$$

$$AnH + Cat: \rightarrow An^{-} + Cat^{+}{-}H \xrightarrow{\text{Pressure}} An^{\bullet} + Cat{-}H^{\bullet}$$

In the first case, as a result of compression, the anion and cation return to their initial radical forms; for example, $Na^+ + Cl^- \rightarrow Na^{\bullet} + Cl^{\bullet}$. In the second case, an onium cation acquires

an electron and does not return in its initial state but forms a radical possessing an intrinsic instability. In vacuum at 0 K, such radicals are kinetically stable, but under finite temperature and pressure these easily release a hydrogen atom and turn to its initial form. To show this process, we have performed an *ab initio* molecular dynamics simulation using the NVT ensemble. Thus, radicals formed from the NH_4^+ cations turn to ammonia and molecular hydrogen (Fig. S3 in the ESI†).

Taking into account the electron transition discussed above, one can assume that conceptual DFT quantities,[45] namely, electronegativity (χ), chemical hardness (η) or electrophilicity (ω) calculated for isolated species (ions or radicals) may be representatives of such a process, like in the case of metal azides (eqn (8)–(10)).[33]

$$\chi = \frac{I + A}{2} \tag{8}$$

$$\eta = I - A \tag{9}$$

$$\omega = \frac{(I + A)^2}{8(I - A)}. \tag{10}$$

Herein, I and A are the ionization energy and electron affinity (in eV), respectively, which can be obtained in terms of vertical approximation (Koopmans' theorem) and as adiabatic energy difference between the corresponding oxidized/reduced and starting form of a species (adiabatic approximation). Recently, we have shown that the latter approach produces ionization energies and proton affinities being close to the experimental ones.[46]

Taking into account that most of the salts in Table 2 bear ammonium and azide ions, we have performed a series of calculations of a few additional ammonium NH_4X and azide XN_3 crystals (salts **66–76**) to track the effect of the counterions X in each series. The corresponding optimized cells and numerical data are presented in Fig. S4 and Table S5 in the ESI.† It becomes clear that dependence exists between q_{100} and χ, and η and ω values for $X^\bullet$, which is more pronounced for the XN_3 series (Fig. S5 in the ESI†). It is important to note that pure cations and anions cannot be applied as representatives of the electron transfer. Indeed, since χ values for alkaline metal ions are extremely high (Table S3 in the ESI†), any difference in $\chi_{Cat} - \chi_{An}$ values with both explosive and non-explosive anions are also too high, which always specify these salts as non-explosive. This can be easily seen from the corresponding I and A values obtained in terms of the vertical approximation for salts **24**, **26**, **32–34**, and **37** (Table S3 in the ESI†).

Thus, we have performed geometry optimization of all radicals formed from ions of salts **1–65** and calculated their χ, η and ω values in terms of vertical and adiabatic approximations (Tables S6 and S7 in the ESI†). Considering the properties of radical pairs we estimate the probability of an inverse process, the salt formation. Naturally, in this case an electron must be detached from a $Cat^\bullet$ and attached to an $An^\bullet$ or equivalently $\chi_{An^\bullet} - \chi_{Cat^\bullet}$; the values obtained in this way are illustrated graphically in Fig. 3. Blue bars indicate those cases,

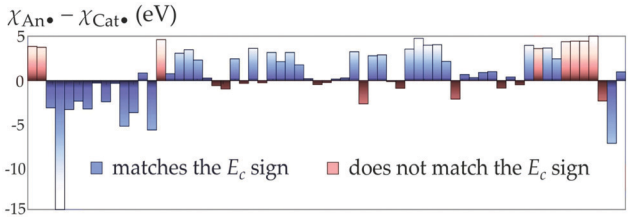

Fig. 3 Differentiation of explosive and non-explosive salts on the basis of electronegativity of the corresponding radicals.

when explosive properties are correctly predicted for salts **1–65**. Conversely, red bars indicate failures of such prediction (21 cases). It is clearly seen, however, that significant errors occur only in 11 cases from the total of 21, while the other values are relatively close to zero, which may be related to the systematic errors of the method of calculation being applied. The other combinations of the conceptual DFT parameters for distinguishing explosive properties of salts **1–65** in terms of both

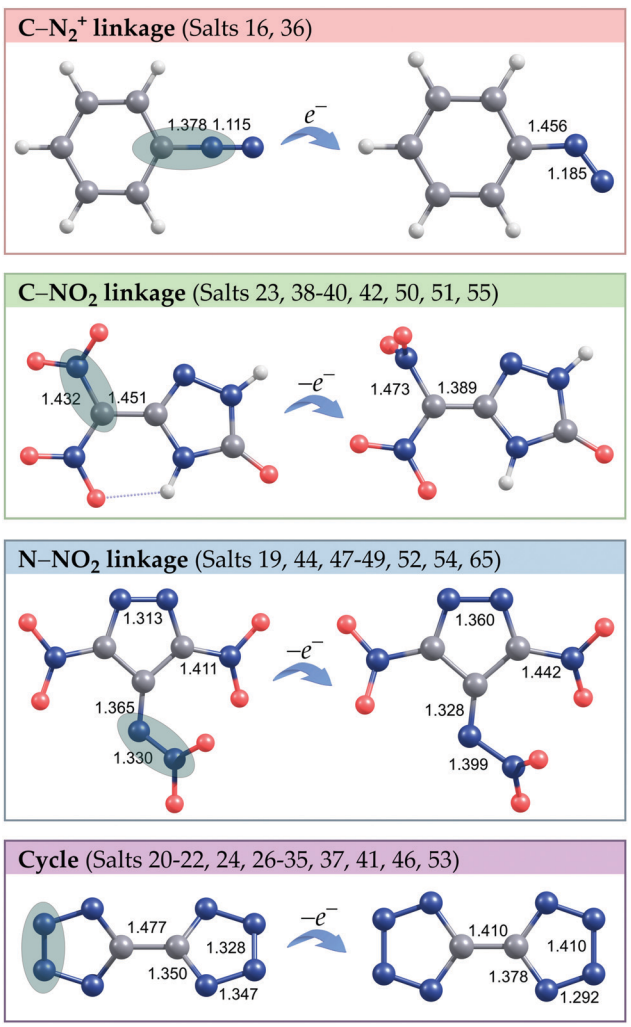

Fig. 4 The changes in explosophore moieties of salts **1–65** caused by the redox process.

This journal is © the Owner Societies 2021

the vertical and adiabatic approximations are presented in Fig. S6 in the ESI.†

We have divided all energetic salts studied in this work into five groups. The first and the largest group is onium (ammonium) salts, which form unstable radicals (Fig. S3 in the ESI†). The other four groups are divided according to their explosophore moieties (Fig. 4). Remarkably, every radical obtained by both the oxidation and reduction demonstrates a significant weakening of the triggering bond, which connects an explosophore group with the rest of the molecule. This is reflected in elongation of the corresponding trigger bonds (Fig. 4).

The relative stability of such radicals may concern the problem of initiation and sensitivity of explosives. Indeed, when an energetic cycle serves as an explosophore, the corresponding salts often demonstrate low impact sensitivity (30–40 J).[47–50] But when another acyclic explosophore is present as a ring substituent, the impact sensitivity usually rises.[51–54] The weakened trigger bonds are then vibrationally destroyed due to the frictionally driven local heating and melting in the hot spots.[55] As a result, the obtained free radicals propagate further chain decomposition of the whole crystal.

Conclusions

Summarizing, we have presented in this paper an interesting and unexpected effect of isotropic compression on ionic charges in crystals of salts, which can be applied for distinguishing explosive and non-explosive materials. The effect is the result of a pressure-driven electron transition from the anion to the cation and the corresponding radical pair formation, which are usually unstable for energetic materials. Taking into account the above-mentioned mechanism, a simple qualitative scheme was proposed for estimation of the energy content, which is based on the difference $\chi_{An^{\bullet}} - \chi_{Cat^{\bullet}}$, which should be positive for energetic salts and *vice versa*. This model was validated on a wide number (76 crystals) of salts including halides, carbonates, sulfate, phosphate, nitrate, tartrate, citrate, sulfonate, alkoxides, ammonium and phosphonium salts, nitroaliphatics, nitrogen-containing heterocycles, pentazoles, aryldiazonia, oxadiazole, azide, *etc.*

Thus, with this paper, a complex pattern of various compression-[34,56] or thermally-induced[57–59] mechanisms of the crystal decomposition is supplemented with another mechanism of the free radical formation in the hot spot. For example, the formation of ABTOX and ammonia during decomposition of TKX-50[57] can be easily understood from the presented electron transfer mechanism. Thus, the latter must be considered as a part of a complex decomposition pattern, which provides its own contribution to the whole mechanism.

Understanding the physical and chemical properties governed by crystal compression or other external energetic perturbation is a crucial factor allowing realization of the strategy of achieving balance between high detonation performance and satisfactory crystal stability.[35,60,61] Of course, the reported effect needs further validation for more families of salts. In particular, it is interesting to track the effect in co-crystals, double salts, *etc.* This should be the content of further studies. One should also keep in mind that in extreme pressure simulations, proton tunneling may come into play and to account for this possibility one should consider alternative crystal sites for protons.[62]

Conflicts of interest

There are no conflicts to declare.

Acknowledgements

This work was supported by the Ministry of Education and Science of Ukraine, Research Fund (Grant No. 0117U003908).

Notes and references

1 X. Dong, A. R. Oganov, G. Qian, X. F. Zhou, Q. Zhu and H. T. Wang, 2015, arXiv: 1503.00230, [cond-mat.mtrl-sci].
2 M. Rahm, R. Cammi, N. W. Ashcroft and R. Hoffmann, *J. Am. Chem. Soc.*, 2019, **141**, 10253–10271.
3 Á. Lobato, H. H. Osman, M. A. Salvadó, P. Pertierra, Á. Vegas, V. G. Baonza and J. Manuel Recio, *Inorg. Chem.*, 2020, **59**, 5281–5291.
4 Q. Sui, X.-T. Ren, Y.-X. Dai, K. Wang, W.-T. Li, T. Gong, J.-J. Fang, B. Zou, E.-Q. Gao and L. Wang, *Chem. Sci.*, 2017, **8**, 2758–2768.
5 B. Schüpp, P. Heines, A. Savin and H.-L. Keller, *Inorg. Chem.*, 2000, **39**, 732–735.
6 W. Denner, H. Schulz and H. d'Amour, *Acta Crystallogr., Sect. A: Cryst. Phys., Diffr., Theor. Gen. Crystallogr.*, 1979, **35**, 360–365.
7 T. Pandey, A. P. Nayak, J. Liu, S. T. Moran, J.-S. Kim, L.-J. Li, J.-F. Lin, D. Akinwande and A. K. Singh, *Small*, 2016, **12**, 4063–4069.
8 R. Mortimer, J. G. Powell and N. Y. Vasanthacharya, *J. Phys.: Condens. Matter*, 1997, **9**, 11209–11218.
9 R. T. Sanderson, *Polar Covalence*, Academic Press, New York, London, 1983.
10 W. J. Mortier, Electronegativity Equalization and its Applications, in *Electronegativity*, ed. K. Das Sen and C. K. Jørgensen, Springer-Verlag, Berlin, Heidelberg, 1987, vol. 66, pp. 125–143.
11 R. Ferreira, *Trans. Faraday Soc.*, 1963, **59**, 1064–1074.
12 P. K. Chattaraj, S. Giri and S. Duley, *J. Phys. Chem. Lett.*, 2010, **1**, 1064–1067.
13 R. Svobodová Vařeková, Z. Jiroušková, J. Vaněk, Š. Suchomel and J. Koča, *Int. J. Mol. Sci.*, 2007, **8**, 572–582.
14 A. Batana and C. Hense, *J. Phys. Chem. Solids*, 1980, **41**, 863–864.
15 A. Batana and J. Faodr, *J. Phys. Chem. Solids*, 1984, **45**, 571–574.
16 S. S. Batsanov, *J. Phys. Chem. Solids*, 1997, **58**, 527–532.
17 S. S. Batsanov, *Russ. J. Phys. Chem.*, 2006, **80**, 135–138.
18 S. S. Batsanov, *J. Struct. Chem.*, 2005, **46**, 306–314.

19 K. Li, Z. Ding and D. Xue, *Phys. Status Solidi B*, 2011, **248**, 1227–1236.
20 D. B. Sirdeshmukh, L. Sirdeshmukh and K. G. Subhadra, *Pramana*, 2007, **69**, 491–520.
21 S. J. Clark, M. D. Segall, C. J. Pickard, P. J. Hasnip, M. J. Probert, K. Refson and M. C. Payne, *Z. Kristallogr. – Cryst. Mater.*, 2005, **220**, 567–570.
22 *Materials Studio 2017*, Dassault Systèmes BIOVIA, San Diego, CA, 2016.
23 J. P. Perdew, K. Burke and M. Ernzerhof, *Phys. Rev. Lett.*, 1996, **77**, 3865–3868.
24 S. Grimme, *J. Comput. Chem.*, 2006, **27**, 1787–1799.
25 G. Kresse and J. Furthmüller, *Phys. Rev. B: Condens. Matter Mater. Phys.*, 1996, **54**, 11169–11186.
26 R. Fletcher, *Practical Methods of Optimization*, Wiley, New York, 1980, vol. 1.
27 C. Fonseca Guerra, J.-W. Handgraaf, E. Jan Baerends and F. Matthias Bickelhaupt, *J. Comput. Chem.*, 2004, **25**, 189–210.
28 M. J. Frisch, G. W. Trucks, H. B. Schlegel, G. E. Scuseria, M. A. Robb, J. R. Cheeseman, G. Scalmani, V. Barone, B. Mennucci and G. A. Petersson, *et al.*, *Gaussian 09, Revision A.02*, Gaussian, Inc., Wallingford, CT, 2009.
29 J.-D. Chai and M. Head-Gordon, *Phys. Chem. Chem. Phys.*, 2008, **10**, 6615–6620.
30 W. J. Hehre, L. Radom, P. v. R. Schleyer and J. A. Pople, *Ab Initio Molecular Orbital Theory*, Wiley, New York, 1986.
31 D. Mathieu and T. Alaime, *J. Phys. Chem. A*, 2014, **118**, 9720–9726.
32 D. Frem, *Combust., Explos. Shock Waves*, 2018, **54**, 704–711.
33 S. V. Bondarchuk, *New J. Chem.*, 2019, **43**, 1459–1468.
34 S. V. Bondarchuk, *J. Phys. Chem. A*, 2018, **122**, 5455–5463.
35 D. Mathieu, *Ind. Eng. Chem. Res.*, 2017, **56**, 8191–8201.
36 D. Li, X. Wu, J. Jiang, X. Wang, J. Zhang, Q. Cui and H. Zhu, *Appl. Phys. Lett.*, 2014, **105**, 071903.
37 X. Wang, J. Li, H. Zhu, L. Chen and H. Lin, *J. Chem. Phys.*, 2014, **141**, 044717.
38 G. Zhang, H. Zhang, S. Ninet, H. Zhu, C. Liu, J.-P. Itie, C. Gao and F. Datchi, *J. Phys. Chem. C*, 2020, **124**, 135–142.
39 D. Li, P. Zhu, J. Jiang, D. Xu, R. Liu, X. Wang, Q. Cui and H. Zhu, *J. Phys. Commun.*, 2017, **1**, 025002.
40 J. Zhang, Z. Zeng, H.-Q. Lin and Y.-L. Li, *Sci. Rep.*, 2014, **4**, 4358.
41 X. Wang, J. Li, J. Botana, M. Zhang, H. Zhu, L. Chen, H. Liu, T. Cui and M. Miao, *J. Chem. Phys.*, 2013, **139**, 164710.
42 N. Yedukondalu, G. Vaitheeswaran, P. Modak and A. K. Verma, *Solid State Commun.*, 2019, **297**, 39–44.
43 G. V. Tikhomirova and A. N. Babushkin, *Phys. Status Solidi B*, 2003, **235**, 337–340.
44 S. V. Bondarchuk, *J. Mol. Graphics Modell.*, 2019, **89**, 114–121.
45 P. Geerlings, F. De Proft and W. Langenaeker, *Chem. Rev.*, 2003, **103**, 1793–1873.
46 S. V. Bondarchuk, *Mol. Syst. Des. Eng.*, 2020, **5**, 1003–1011.
47 Y. Xu, L. Tian, D. Li, P. Wang and M. Lu, *J. Mater. Chem. A*, 2019, **7**, 12468–12479.
48 Z.-B. Zhang, J.-G. Zhang and M. Gozin, *ChemistrySelect*, 2018, **3**, 3463–3473.
49 Y. Shang, B. Jin, Q. Liu, R. Peng, Z. Guo and Q. Zhang, *J. Mol. Struct.*, 2017, **1133**, 519–525.
50 N. Fischer, D. Fischer, T. M. Klapötke, D. G. Piercey and J. Stierstorfer, *J. Mater. Chem.*, 2012, **22**, 20418–20422.
51 Y.-H. Joo and J. M. Shreeve, *Chem. – Eur. J.*, 2009, **15**, 3198–3203.
52 N. Szimhardt, M. F. Bölter, M. Born, T. M. Klapötke and J. Stierstorfer, *Dalton Trans.*, 2017, **46**, 5033–5040.
53 Y. Tang, J. Zhang, L. A. Mitchell, D. A. Parrish and J. M. Shreeve, *J. Am. Chem. Soc.*, 2015, **137**, 15984–15987.
54 H. Li, F.-Q. Zhao, B.-Z. Wang, L.-J. Zhai, W.-P. Lai and N. Liu, *RSC Adv.*, 2015, **5**, 21422–21429.
55 S. V. Bondarchuk, *CrystEngComm*, 2018, **20**, 5718–5725.
56 Z. Zheng and J. Zhao, *J. Chin. Phys. B*, 2016, **25**, 076202.
57 N. V. Muravyev, K. A. Monogarov, A. F. Asachenko, M. S. Nechaev, I. V. Ananyev, I. V. Fomenkov, V. G. Kiselev and A. N. Pivkina, *Phys. Chem. Chem. Phys.*, 2017, **19**, 436–449.
58 Z. Lu and C. Zhang, *J. Phys. Chem. C*, 2017, **121**, 21252–21261.
59 Q. An, W.-G. Liu, W. A. Goddard, III, T. Cheng, S. V. Zybin and H. Xiao, *J. Phys. Chem. C*, 2014, **118**, 27175–27181.
60 C. Li, H. Li, H.-H. Zong, Y. Huang, M. Gozin, C. Q. Sun and L. Zhang, *iScience*, 2020, **23**, 100944.
61 H. Li, L. Zhang, N. Petrutik, K. Wang, Q. Ma, D. Shem-Tov, F. Zhao and M. Gozin, *ACS Cent. Sci.*, 2020, **6**, 54–75.
62 R. Méreau, D. Mathieu, M. Elstner and T. Frauenheim, *Phys. Rev. B: Condens. Matter Mater. Phys.*, 2004, **69**, 104101.

This journal is © the Owner Societies 2021